nature neuroscience

Lag normalization in an electrically coupled neural network

Stuart Trenholm[1], David J Schwab[2], Vijay Balasubramanian[3,4] & Gautam B Awatramani[1]

Moving objects can cover large distances while they are processed by the eye, usually resulting in a spatially lagged retinal response. We identified a network of electrically coupled motion–coding neurons in mouse retina that act collectively to register the leading edges of moving objects at a nearly constant spatial location, regardless of their velocity. These results reveal a previously unknown neurophysiological substrate for lag normalization in the visual system.

In the mammalian retina, there are four types of ON-OFF directionally selective ganglion cells (DSGCs), each preferentially responding to edges moving in a specific cardinal direction[1,2]. These cells exhibit low background activity and initiate precise spiking patterns in response to movement, such that the very first spikes that they generate register information about the spatial location of edges[3]. In addition, their peak firing rates provide information about stimulus velocity[1,4]. In the rabbit retina, a subpopulation of DSGCs is homologously coupled via gap junctions[5]. In the mouse retina, this population corresponds to the upward coding DSGCs, identified in the *Hb9* (also known as *Mnx1*)-*eGFP* transgenic line[6]. We compared the response properties of coupled and uncoupled ON-OFF DSGCs, applying two-photon assisted patch-clamp techniques in an isolated whole-mount retinal preparation.

We first compared the locations where DSGCs initially detected the leading edge of white bars (300 × 300 µm, 96% Weber contrast) moving at 600 µm s^{-1} in the direction that elicited the maximal response (that is, the preferred direction). Uncoupled DSGCs began responding just as the leading edge of the moving bar entered their dendritic fields (20 ± 9 µm into the dendritic field; **Fig. 1a**), consistent with their established receptive field properties[7]. In contrast, coupled (*Hb9*$^+$) DSGCs initiated spiking 106 ± 16 µm, on average, before the stimulus edge reached their dendritic fields ($n = 9$, $P < 0.005$; **Fig. 1a**; n represents number of cells in all cases). Given that the different subtypes of DSGCs receive inputs from the same set of presynaptic bipolar/starburst amacrine cells[2,8], the early responses observed in coupled DSGCs suggest that activity in neighboring pre-junctional cells effectively propagates through dendritic gap junctions[9]. Furthermore, as *Hb9*$^+$ DSGCs possessed starkly asymmetric dendritic trees[6] (**Fig. 1a**), it appears that lateral electrical inputs partially compensated for the lack of dendrites on the preferred side of the soma.

The most unexpected aspect of edge registration was revealed when we compared the position at which spikes were initiated when bars were presented at different velocities (150–1,800 µm s^{-1}). Uncoupled DSGCs detected the leading edges of moving bars at positions that systematically shifted in space as a function of the stimulus velocity. This spatial lag[10–14] was consistent with an apparent delay (t_d) of 99 ± 11 ms between the time when images fell on photoreceptors and the initiation of DSGC spiking responses (**Fig. 1b**,**c**). For uncoupled DSGCs at the fastest speed tested (1,800 µm s^{-1}), responses initiated only after the moving edge had nearly crossed the entire dendritic field (81 ± 10 µm past the soma, $n = 12$). In contrast, coupled DSGCs detected edges at a nearly constant retinal location (114 ± 9 µm before the soma, $n = 15$) regardless of stimulus velocity (**Fig. 1b**,**c**). This lag normalization was apparent for both positive and negative contrast stimuli (**Supplementary Fig. 1**), suggesting that it did not require specific elements of the ON or OFF presynaptic pathways that provide inputs to DSGCs (for simplicity, we focused on positive contrasts). Thus, gap junction coupling appears to endow DSGCs with a unique ability to compensate for processing delays that occur in the feedforward retinal circuits.

In contrast to the initial responses to moving edges, the properties of the peak firing rates were similar in coupled and uncoupled DSGCs. In both cell types, peak responses spatially lagged the true positions of the moving edges (**Fig. 1b**,**c**) and increased in amplitude as a function of velocity (**Supplementary Fig. 2**). In coupled DSGCs, as only the initial response was lag normalized and not the peak, their response waveforms were skewed toward the leading edge (average skewness = –0.38 ± 0.02, $n = 15$; **Fig. 1b**; this waveform was not substantially distorted by the convolution filtering used to define instantaneous firing rates from the raw spikes; **Supplementary Fig. 3**). In contrast, in uncoupled DSGCs, both the initial and peak responses were equally lagged, resulting in responses that were significantly more symmetrical (average skewness = 0.07 ± 0.07, $n = 12$, $P = 0.029$; **Fig. 1b**). We hypothesized that the lag uncorrected peak component arose from chemical synapses mediated by bipolar/starburst amacrine cells that stimulate coupled and uncoupled DSGCs alike, whereas the lag normalized response onset of coupled DSGCs arose from activity in upstream pre-junctional ganglion cells.

To understand the nature of lateral gap junction–mediated excitation, we next assessed the input contributions from a single neighboring DSGC. To do so, we made simultaneous measurements of extracellular spiking from pre-junctional DSGCs and excitatory postsynaptic currents (EPSCs) in voltage-clamped post-junctional DSGCs (V_{HOLD} ~–60 mV, 5 mM QX-314 was included in the recording pipette to block axonal and dendritic Na^+ channels[15]; **Fig. 2a**). Spikes generated in pre-junctional cells were always followed closely by low-amplitude spikelets in the post-junctional cell (average amplitude = 30 ± 2 pA, average latency = 0.37 ± 0.3 ms, $n = 6$; **Fig. 2a**). Thus, coupled DSGCs begin to receive excitation from a considerable distance away, when the first

[1]Department of Biology, University of Victoria, Victoria, British Columbia, Canada. [2]Department of Physics, Princeton University, Princeton, New Jersey, USA. [3]David Rittenhouse Laboratory, University of Pennsylvania, Philadelphia, Pennsylvania, USA. [4]Laboratoire de Physique Théorique, Ecole Normale Supérieure, Paris, France. Correspondence should be addressed to G.B.A. (gautam@uvic.ca).

Received 5 November 2012; accepted 13 December 2012; published online 13 January 2013; doi:10.1038/nn.3308

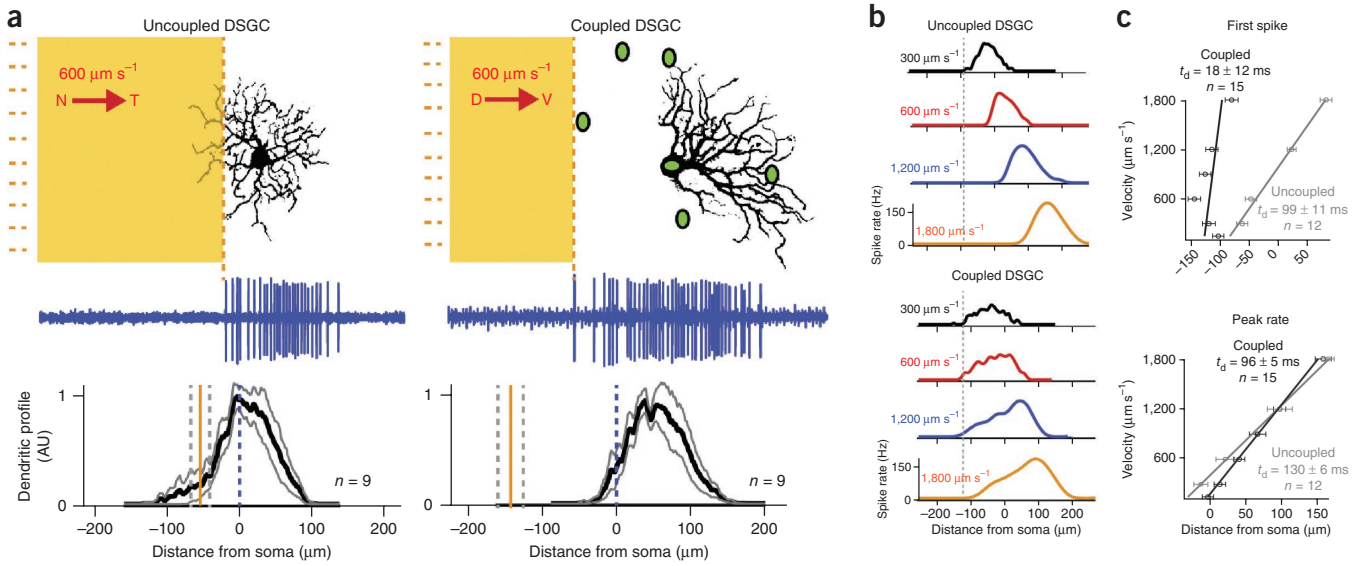

Figure 1 Lag normalization in the electrically coupled population of upward coding ON-OFF DSGCs. (**a**) A snapshot of moving light bars (600 µm s^{-1}) shown in relation to the ON dendrites of uncoupled (left) and coupled (right) DSGCs at positions where the spiking responses initiated. The entire ON spiking response (blue trace), after the stimulus edge crossed the entire receptive field, is illustrated. The average start position (vertical orange line, ± s.e.m. indicated by gray dashed lines) and the average ON dendritic profiles are shown below (black traces, ± s.e.m. indicated by gray traces; the position of the soma is indicated by the blue dashed line; see Online Methods). Green ellipses (top right) represent the somata of neighboring GFP$^+$ DSGCs in the *Hb9-eGFP* transgenic mouse retina. D, dorsal; N, nasal; T, temporal; V, ventral. (**b**) Plotting the waveform of spike activity triggered by bars moving at the indicated velocities in relation to the position of the leading edge of the stimulus reveals spatially lagged responses in uncoupled (top), but not coupled (bottom), DSGC. For all traces, the leading edge of the stimulus is at the soma at 0 µm. The gray dashed lines indicate the position of the leading edge where responses initiated at the slowest velocity tested. (**c**) The positions of the leading edge when the first spike (top) and the peak spiking response (bottom) were observed, plotted as a function of velocity for uncoupled and coupled DSGCs. The inverse slope of the linear fit provides an estimate of the apparent time delay (t_d), which is proportional to the spatial lag (for perfect lag normalization, t_d = 0 ms delay). Error bars represent s.e.m.

anticipatory spikes are generated in the upstream DSGC. That the initial coupling-mediated inputs occurred much farther from the soma than the first spikes suggests that coupled inputs alone do not drive spike activity in post-junctional cells. Thus, gap junction inputs are likely to become effective when they are summed with inputs from other ganglion and/or bipolar cells. Such contextual restraints on gap junction signaling could allow for strong anticipatory signals to develop without leading to run-away excitation in the network.

As the measured spikelet currents only represent the fast component of the gap junction–mediated priming signal, the total gap junction input is expected to be larger. Indeed, spiking responses and EPSCs of coupled DSGCs had a distinct slow rising component that was not observed in uncoupled DSGCs (EPSC τ_{rise} = 118 ± 11 ms for coupled and 66 ± 5 ms for uncoupled DSGCs, n = 11 for coupled and 10 for uncoupled DSGCs, P = 0.029; **Fig. 2b–d**). Consistent with a role for gap junctions in the early response component of coupled DSGCs, the initial phase of both EPSCs and spiking responses were selectively inhibited in the presence of the gap junction antagonist 18β-glycyrrhetinic acid (25 µM 18βGA; for spiking responses, Δ = 60 ± 8 µm, n = 12, P < 0.001; for EPSCs, Δ = 125 ± 31 µm, n = 5, P = 0.01; **Fig. 2b**,**c**, whereas the responses of uncoupled DSGCs were not significantly affected (n = 4, P > 0.05; **Fig. 2d**). Together, these results indicate an important role for pre-junctional DSGCs in controlling the initiation of spiking responses in their downstream neighbors via gap junctions.

Next, we sought to understand how converging electrical and chemical synaptic inputs result in lag normalization in the network. To compensate for spatial response lags that increase linearly with velocity, the strength of the lateral priming must increase in parallel. Indeed, signals mediated through gap junctions are expected to get larger with stimulus velocity because the peak firing rate of DSGCs

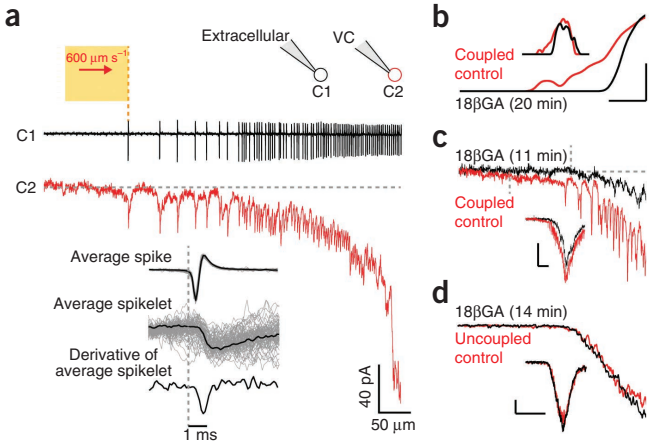

Figure 2 Gap junctions between upward coding DSGCs mediate lateral excitation. (**a**) Responses to the leading edge of a bar moving at 600 µm s^{-1}, measured simultaneously from neighboring GFP$^+$ DSGCs. Spike trains are shown from the pre-junctional DSGC (C1, black) and EPSCs in the post-junctional DSGC (C2, red). Yellow bar indicates position of stimulus at the position where the first spike was generated in C1. Inset: average pre-junctional spike, spike-triggered post-junctional current (average spikelet) and the derivative of the post-junctional current (raw data for 50 consecutive spikes or spikelets are shown in gray). (**b**,**c**) Response onsets of coupled DSGCs before and after the application of the gap junction antagonist 18βGA, 25 µM (the entire ON response waveforms are shown in the insets). (**d**) Responses of uncoupled DSGCs were not affected by application of 18βGA. Vertical dashed lines in **c** indicate the start of EPSCs in control and drug conditions. Vertical and horizontal scale bars represent 50 µm and 40 Hz (**b**), 250 µm and 100 Hz (**b**, inset), 12 µm and 25 pA (**c**), 100 µm and 100 pA (**c**, inset), 50 µm 50 pA (**d**), and 75 µm and 250 pA (**d**, inset).

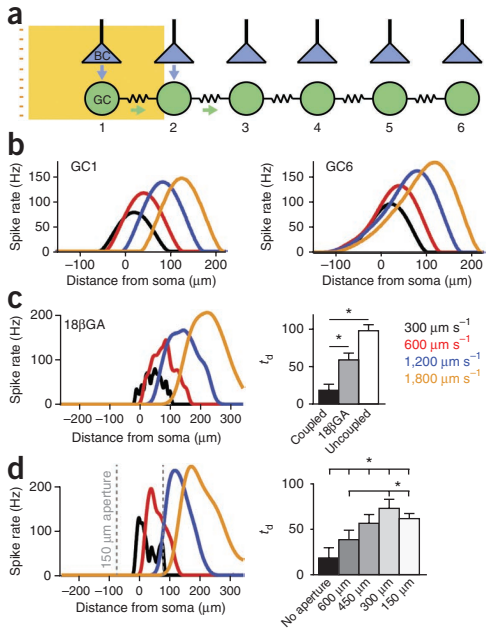

Figure 3 Serial interactions between multiple electrically coupled DSGCs are required for lag normalization. (**a**) Model schematic: an array of coupled ganglion cells (GCs) was stimulated by feedforward currents from bipolar cells (BCs) with experimentally measured receptive fields and velocity-dependent response amplitudes. The total current into the *n*th ganglion cell is the sum of the bipolar cell input and scaled gap junction input from the preceding ganglion cell (see Online Methods). Lag normalization is achieved by tuning the effective gap junction coupling strength to best fit the data. (**b**) Numerical simulation with different stimulus velocities shows that lag-normalized responses developed by the sixth GC (GC6) in the chain. (**c**) Lag normalization, measured experimentally, was inhibited by the gap junction antagonist 18βGA (25 μM, $P = 0.017$, $n = 4$). The average apparent delay (t_d) is plotted for the indicated conditions. (**d**) Lag normalization, but not response amplitude, was reduced when stimuli were presented through a 150-μm aperture. The apparent delay (t_d) is plotted as a function of the diameter of the aperture (right). $^*P < 0.05$ for the indicated pairwise comparisons. Error bars, s.e.m.

increases with velocity (**Supplementary Fig. 2**). Moreover, as gap junctions cause the responses of coupled ganglion cells to be shifted, these shifted responses in turn provide an even earlier priming signal to their downstream neighbors. Thus, priming signals compound over the network. To test whether such effects could produce lag normalization, we modeled an array of *N* coupled ganglion cells (**Fig. 3a**,**b**) stimulated by experimentally measured velocity-dependent bipolar cell inputs (Online Methods). The coupling strength between ganglion cells was the only required tuneable variable in the model. In addition, previously described gain control mechanisms[10,16] were also implemented (Online Methods). The first cell in the array (GC1) did not have any upstream coupled neighbors and did not exhibit lag normalization (**Fig. 3b**). However, the ability to normalize spatial lag built up in subsequent DSGCs and reached a steady state by the sixth cell (**Fig. 3b**). Thus, a minimal model with a single tuneable parameter (the effective electrical coupling strength between DSGCs) captures the most salient response features of coupled DSGCs and suggests that lag normalization is a cooperative effect requiring serial gap junction interactions between several DSGCs.

To experimentally test the insights from our model, we first confirmed the role of gap junctions in lag normalization using pharmacology and found that it was significantly impaired in the presence of 25 μM 18βGA ($n = 4$, $P = 0.017$; **Fig. 3c**). To examine how signals compounded over the network, we limited the area of retina being stimulated by presenting moving stimuli through an aperture of variable size (diameter 150–600 μm, centered over the soma; **Fig. 3d**). When the light stimulus was restricted over the dendritic field (150-μm aperture), peak spiking responses were left intact, but lag normalization was greatly diminished ($n = 5$, $P < 0.03$; **Fig. 3d**). However, as the aperture was made larger and upstream DSGCs were stimulated, lag normalization progressively increased. When stimuli approached from >300 μm upstream of the soma (that is, 3–4 DSGC somata away), lag normalization was restored to control levels (**Fig. 3d**). Thus, the effects of electrical signaling compound over extended areas, implicating a cooperative, serial interaction between electrically coupled DSGCs in the generation of lag normalization, as predicted by our model.

Our results describe a retinal circuit that uses gap junction coupling between neighboring upward-coding DSGCs to correct for velocity-dependent spatial response lags that arise from processing delays[10–14]. Lag normalization arose when each cell in a chain of electrically coupled cells primed its downstream neighbors to fire earlier, partly by exploiting and amplifying the velocity dependence of the single-cell response dynamics. This previously unknown collective phenomenon could also be implemented in other specialized ganglion cells[17,18] (**Supplementary Fig. 4**) or even in other sensory circuits that need to compensate for neural delays.

METHODS

Methods and any associated references are available in the online version of the paper.

Note: Supplementary information is available in the online version of the paper.

ACKNOWLEDGMENTS

We thank W.H. Baldridge, B. Chow and K.R. Delaney for comments, K. Johnson for writing routines in Matlab and Z. Shi for maintaining mouse colonies. This work was supported in part by US National Science Foundation PHY-1058202 and EF-0928048 (V.B.) and was completed at the Aspen Center for Physics, which is supported by National Science Foundation PHY-1066293. This work was also supported by Canadian Institutes of Health Research 342202-2007 and Foundation for Fighting Blindness (Canada) (G.B.A.).

AUTHOR CONTRIBUTIONS

All experiments were performed and analyzed by S.T. and were designed by S.T. and G.B.A. The computational model was developed by D.J.S., V.B. and G.B.A. The paper was written by S.T., V.B. and G.B.A.

COMPETING FINANCIAL INTERESTS

The authors declare no competing financial interests.

Published online at http://www.nature.com/doifinder/10.1038/nn.3308.
Reprints and permissions information is available online at http://www.nature.com/reprints/index.html.

1. Barlow, H.B., Hill, R.M. & Levick, W.R. *J. Physiol.* (*Lond.*) **173**, 377–407 (1964).
2. Vaney, D.I., Sivyer, B. & Taylor, W.R. *Nat. Rev. Neurosci.* **13**, 194–208 (2012).
3. Gollisch, T. & Meister, M. *Science* **319**, 1108–1111 (2008).
4. Oyster, C.W. *J. Physiol.* (*Lond.*) **199**, 613–635 (1968).
5. Vaney, D.I. *J. Neurosci.* **14**, 6301–6316 (1994).
6. Trenholm, S., Johnson, K., Li, X., Smith, R.G. & Awatramani, G.B. *Neuron* **71**, 683–694 (2011).
7. Yang, G. & Masland, R.H. *J. Neurosci.* **14**, 5267–5280 (1994).
8. Wassle, H., Puller, C., Muller, F. & Haverkamp, S. *J. Neurosci.* **29**, 106–117 (2009).
9. Vervaeke, K., Lorincz, A., Nusser, Z. & Silver, R.A. *Science* **335**, 1624–1628 (2012).
10. Berry, M.J. II, Brivanlou, I.H., Jordan, T.A. & Meister, M. *Nature* **398**, 334–338 (1999).
11. Krekelberg, B. & Lappe, M. *Trends Neurosci.* **24**, 335–339 (2001).
12. Nijhawan, R. *Nature* **370**, 256–257 (1994).
13. Nijhawan, R. *Trends Cogn. Sci.* **6**, 387 (2002).
14. Anderson, C.H. & Van Essen, D.C. *Proc. Natl. Acad. Sci. USA* **84**, 6297–6301 (1987).
15. Oesch, N., Euler, T. & Taylor, W.R. *Neuron* **47**, 739–750 (2005).
16. Shapley, R.M. & Victor, J.D. *J. Physiol.* (*Lond.*) **285**, 275–298 (1978).
17. Völgyi, B., Chheda, S. & Bloomfield, S.A. *J. Comp. Neurol.* **512**, 664–687 (2009).
18. Bloomfield, S.A. & Volgyi, B. *Nat. Rev. Neurosci.* **10**, 495–506 (2009).

ONLINE METHODS

All procedures were performed in accordance with the Canadian Council on Animal Care and were approved by the University of Victoria's Animal Care Committee and carried out in adult wild-type (C57Bl/6) and *Hb9-eGFP* transgenic mice, as described previously[6]. Mice were dark adapted for 30 min before being killed and retinas were dissected using infrared goggles. All reagents were purchased form Sigma-Aldrich Canada unless otherwise noted.

Physiological recordings. Extracellular spike recordings were made in cell-attached patch-clamp configuration using 5–10-MΩ electrodes filled with Ringer's solution. Voltage-clamp whole-cell recordings were made using 4–7-MΩ electrodes containing 112.5 mM CH_3CsO_3S, 1 mM $MgSO_4$, 10 mM EGTA, 10 mM HEPES, 4 mM ATP-Mg_2, 0.5 mM GTP-Na_3, 5 mM QX-314, 7.75 mM Neurobiotin (Vector Labs) and 0.25 mM Alexa 594 (Invitrogen). The pH was adjusted to 7.4 with CsOH. The reversal potential for chloride was calculated to be near –70 mV. The junction potential for the intracellular solution was ~10 mV and was left uncorrected. Recordings were made with a MultiClamp 700B amplifier (Molecular Devices). Signals were digitized at 10 kHz using a BNC-2090A A/D board (National Instruments) and acquired using custom software written in LabVIEW (D. Balya, Friedrich Meischer Institute). GFP^+ neurons in the *Hb9-eGFP* transgenic retina were visually targeted using two-photon laser-scanning microscopy (950 nm). GFP^- DSGCs were identified by their soma size and directionally selective response properties. Dendritic morphologies were imaged at 850 nm after individual neurons were loaded with Alexa 594. Dendritic morphologies were reconstructed and analyzed in ImageJ (http://rsbweb.nih.gov/ij/). Dendritic profiles (**Fig. 1**) were estimated by measuring the total fluorescence after collapsing the entire image in the axis perpendicular to that of the moving stimulus.

Light stimulus. Light stimuli were presented with a Digital Light Processing (DLP) projector (Hitachi Cpx1, refresh rate = 75 Hz) and controlled with custom software. The ambient background intensity, as measured with a calibrated spectrophotometer (USB2000, Ocean Optics) was 3×10^{12} photons s^{-1} cm^{-2} (sampled at 500 nm), which is equivalent to 400 photoisomerizations $cone^{-1}$ s^{-1}. Light stimuli were projected from below the specimen and were focused on the outer segments of the photoreceptors using the substage condenser. The preferred direction for DSGCs was calculated after presenting stimuli in eight directions over each cell. We found that lag normalization was most robust after adapting the retinal preparation for 30 min with constant light (400 photoisomerizations $cone^{-1}$ s^{-1}) before physiological recordings, which may result from increased ganglion cell coupling[19].

Analysis of physiological data. The spike rate was estimated by low-pass filtering the spike train via convolution with a Gaussian kernel with a fixed width, σ = 25 ms. The skewed response waveform of coupled DSGCs remained largely constant as σ was varied between 5 and 50 ms, indicating that filtering methods did not introduce biases in the spike rate measurements (**Supplementary Fig. 3**). To depict where spikes are registered in space, we plotted spike rates as a function of the position of the leading edge of the stimulus. All spiking data represent averages of 2–4 trials (unless otherwise indicated). Skewness for the ON response spike waveforms was computed as the third moment divided by the second moment raised to the 3/2 power. Negative values correspond to leftward skew. Comparisons between groups were made with *t* tests. Comparisons made in recordings from the same cell before and after applying pharmacological agents were made using paired *t* tests. For data that failed normality tests, we used the Mann-Whitney rank sum test instead of *t* tests and the signed rank test instead of paired *t* tests. Data are presented as mean ± s.e.m.

Model of DSGC network. To understand how the network of coupled DSGCs collectively works to normalize spatial lag, we constructed a simplified computational model with a linear array of ganglion cells (GC_1, GC_2,…GC_n) spaced Δ = 75 µm apart (reflecting the approximate spacing of cells[6]). The current input into the *n*th ganglion cell (I_n) was taken to be

$$I_n(t) = J_n(t) + \alpha\, I_{n-1}(t) \tag{1}$$

where J_n is the feedforward input from the bipolar cells, I_{n-1} is the current in the preceding ganglion cell in the array, and α is a parameter reflecting the net strength of gap junction coupling between cells *n – 1* and *n*. The proportionality constant $0 < \alpha < 1$ is the only free parameter and captures the effective strength of the ensemble of gap junctions that couple a pair of cells (**Fig. 3** defines $\alpha = e^{-\beta}$). Our data (**Fig. 1c** and **Supplementary Fig. 3**) revealed that coupled DSGC responses were skewed toward the side from which the stimulus was approaching, suggesting that downstream cells were not as effective at driving spikes in upstream cells, likely reflecting offset inhibition and suppressive gain control. For example, offset inhibition implies that the inhibitory input to a DSGC will overlap with excitatory gap junction input from downstream cells, suppressing the priming effect provided by the latter. We modeled this effect approximately by allowing current in cell *i – 1* to contribute to the current in cell *i* (weighted by the effective coupling α), while the cell *i + 1* did not influence the current in cell *i* (that is, offset inhibition and suppressive gain control are taken to entirely suppress the effects of possible priming signals from downstream cells). To keep the model simple, we also neglected time delays in gap junction transmission.

Iterating equation (1) gives an equation relating the current in cell *n* to the bipolar cell input channeled through the previous ganglion cells in the array

$$I_n(t) = \sum_{m=1}^{n} \alpha^{n-m} J_m(t) \tag{2}$$

We estimated the spatial receptive field giving rise to the excitatory currents J_m by fitting EPSCs experimentally measured in uncoupled DSGCs as a function of bar position (data not shown) with a Gaussian (s.d. δ = 58.5 µm). The velocity-dependent maximum amplitude $g(v)$ of the current J_m was taken directly from measurements in uncoupled cells (data not shown). Thus, when a bar with a trajectory $x(t) = vt$ moved over our model network of DSGCs, the bipolar input to the *m*th ganglion cell was described by

$$J_m(t) = g(v) \exp\left[-\frac{\left(x(t-\tau) - m\Delta\right)^2}{2\delta^2} \right] \tag{3}$$

where $g(v)$ is the measured velocity-dependent response amplitude, $x(t) = vt$ is the stimulus edge trajectory, $\tau \sim 70$ ms is a fixed transmission delay between the retinal input and the ganglion cells (reflecting a typical effective delay in uncoupled cells), Δ = 75 µm is the spacing between neighboring ganglion cells, and δ = 58.5 µm is the measured s.d. of the receptive field.

The sum in equation (2) can be evaluated numerically and passed through a spike generator (see below and **Fig. 3**), but it is insightful to first carry out an approximate analytic calculation to determine the qualitative features of the model. To do so, we observed that, as equation (2) is a sum of Gaussians multiplied by a decaying exponential, it will be dominated by the largest term in the sum, provided that the s.d. δ and the coupling α are relatively small. We can find the largest term by differentiating the summands $\alpha^{n-m} J_m$ with respect to *m* and requiring the derivative to equal zero. This determines the index of the largest summand to be

$$m^* = \frac{\beta\delta^2}{\Delta^2} + \frac{x(t-\tau)}{\Delta} \tag{4}$$

where we have defined the logarithm of the coupling $\beta = -\ln\alpha$. More precisely, the index of the largest summand is the integer closest to m^*. This treatment applies when the coupling α is large enough; otherwise $m^* = n$. Note also that $\beta > 0$, as $0 < \alpha < 1$. Thus, in this approximation, we write

$$I_n(t) \approx \alpha^{n-m^*} J_{m^*}(t) \tag{5}$$

To find the position of the stimulus when the *nth* ganglion cell begins spiking, we then set $I_n(t) = C$, where *C* is the current threshold for spiking.

Solving the equation $I_n(t) = C$ in our approximation determines that the *n*th DSGC in our model array starts spiking when the stimulus edge is at a location x^* determined by

$$x^* - n\Delta = v\tau - \frac{\Delta}{\beta} \ln\left(\frac{g(v)}{C}\right) - \frac{\beta\,\delta^2}{2\Delta} \tag{6}$$

The left-hand side of equation (6) gives the position of the stimulus relative to the receptive field center of the *n*th ganglion cell. The first term on

doi:10.1038/nn.3308

the right-hand side (RHS), $v\tau$, is a velocity-dependent spatial lag that arises from the fixed time delay τ due to slow signal transduction. The third term on the RHS, $K = \beta\delta^2/2\Delta$, gives a velocity-independent shift. The second term on the RHS provides a velocity-dependent shift and is negative, as $\beta > 0$ and $g(v) > C$ for suprathreshold responses. Thus, in a range of velocities for which $g(v) \sim \exp(\gamma v)$ the gap junction coupling $\beta = -\ln\alpha$ can be tuned to cancel the term $v\tau$ and thus achieve perfect lag normalization. Of course, in detail, $g(v)$ cannot be exponential and saturates at high velocities. We observed from **Figure 1** that the spatial lag is almost perfectly normalized for the first and third of the tested velocities (300 and 1,200 μm s^{-1}). If we consider the $g(v)$ for these two velocities as being fit by an exponential, our model predicts overcompensation of the lag at intermediate velocities (because of the super-exponential values of $g(v)$) and undercompensation at high velocities (as a result of subexponential growth of $g(v)$). Precisely this pattern was seen in our data.

To more fully capture lag normalization in our model and to correctly reproduce any constant shifts in the location of the stimulus which first evokes responses, we numerically summed equation (2) to determine the input current into the nth cell in the array. Spike rates were calculated by passing the input current through a threshold linear rectifier. That is, when input current was below the threshold $C = 100$ pA, the spike rate was zero. Above threshold, the spike rate was taken to increase linearly with input current with a proportionality coefficient of 0.7. The spike rate parameters were set to best reproduce the response amplitudes of uncoupled ganglion cells in our data for a range of stimulus velocities. This simple model captures the essential features of lag normalization as seen in our data.

To further refine our model, we added dynamic gain control $g(t)$ to the gap junction synapses in the model network[4]. Gap junction signals were exponentially filtered and then passed through a sigmoidal nonlinearity to arrive at a multiplicative gain factor, which was applied to subsequent gap junction input. Briefly, the dynamics are described by the equation[10,16]

$$\frac{dg_n(t)}{dt} = -\frac{1}{\tau_g} g_n(t) + \lambda I_n(t) \tag{7}$$

where the constants $\tau_\Gamma = 17$ ms and $\lambda = 0.0002$ were selected to obtain the best fit to the experimentally observed peak firing rates of coupled DSGCs, and the subscript n refers to the nth cell. The sigmoidal nonlinearity is described by replacing the static coupling α by

$$\alpha^*(t) = \alpha \frac{K^4}{K^4 + g_n(t)^4} \tag{8}$$

with $K = 3.5$. The coupling strength $\alpha = 0.63$ was fit to best reproduce the experimental spike onset locations, x^*, of coupled cells. The model required an array of approximately five cells to establish a stable response profile, similar to what was observed in our masking experiments (**Fig. 3**). In addition to reproducing lag normalization, the model with gain control also correctly predicted the spatial offset (that is, skewness) in the response and is included in the text (**Fig. 3**).

19. Hu, E.H., Pan, F., Volgyi, B. & Bloomfield, S.A. *J. Physiol.* **588**, 4145–4163 (2010).